

Spectral Decomposition of Missing Transverse Energy at Hadron Colliders

Kyu Jung Bae,^{1,*} Tae Hyun Jung,^{1,†} and Myeonghun Park^{1,2,‡}

¹Center for Theoretical Physics of the Universe,
Institute for Basic Science (IBS), Daejeon, 34051, Korea
²School of Liberal Arts, Seoul-Tech, Seoul 139-743, Korea

(Dated: June 14, 2017)

We propose a spectral decomposition to systematically extract information of dark matter at hadron colliders. The differential cross section of events with missing transverse energy (\cancel{E}_T) can be expressed by a linear combination of basis functions. In the case of s -channel mediator models for dark matter particle production, basis functions are identified with the differential cross sections of subprocesses of virtual mediator and visible particle production while the coefficients of basis functions correspond to dark matter invariant mass distribution in the manner of the Källén-Lehmann spectral decomposition. For a given \cancel{E}_T data set and mediator model, we show that one can differentiate a certain dark matter-mediator interaction from another through spectral decomposition.

Introduction Cosmological and astrophysical observations have seen strong clues of dark matter (DM) from its gravitational interaction. For its observed thermal relic density, DM particles are believed to have non-gravitational interactions with the Standard Model (SM) particles, for example, weakly interacting massive particles [1, 2]. In order to probe such DM particles, many experiments have been conducted [3, 4].

Understanding DM production processes at colliders is of great importance for the investigation of DM annihilation in the early Universe due to the time reversal symmetry [5]. To identify interactions between DM and SM particles, many studies have utilized initial state radiation (ISR) with a missing (transverse) energy at linear colliders [6, 7] and the Large Hadron Collider (LHC) [8, 9].

Here we point out that one of the best ways to analyze DM signals at colliders is to reconstruct DM invariant mass ($m_{\chi\chi}$) distributions. By looking at $m_{\chi\chi}$ distribution, we can extract many properties of dark sector: e.g., masses and spins of DM particles and information about the mediator(s). In the case of a linear collider, we know the initial energy and momentum, so we are able to reconstruct $m_{\chi\chi}$ from the recoil energy, $m_{\chi\chi}^2 = (P_0 - \sum_{\text{vis}} P_{\text{vis}})^2$ where $P_0 = (E_{\text{CM}}, \vec{0})$ is the initial four momentum and P_{vis} are four momenta of outgoing visible particles. In contrast, the $m_{\chi\chi}$ reconstruction is not available at hadron colliders due to the ignorance of initial beam-directional momentum P_z of incoming partons. Alternatively, we can utilize transverse momenta of visible particles to reconstruct a missing transverse energy, $\cancel{E}_T = |\sum_{\text{vis}} \vec{P}_{\text{vis}}^T|$ where \vec{P}_{vis}^T 's are transverse components of three momenta of visible particles. For this reason, previous studies of analyzing DM signals at hadron colliders had to rely on the template fitting method simulated by Monte Carlo (MC) tools which maps models to the \cancel{E}_T distribution. However, this approach is highly model dependent. To cover various DM models, we need to generate corresponding MC simulations for each DM scenario.

In this letter, we propose a spectral decomposition to

extract $m_{\chi\chi}$ distribution at hadron colliders from the \cancel{E}_T distribution. Spectral decomposition has been used in various fields. One of the most famous examples is Fourier transformation, the decomposition of a function into the linear combination of sinusoidal functions. In a similar way, we define proper basis functions and decompose the \cancel{E}_T distribution into the linear combination of basis functions. The coefficients correspond to the DM invariant mass distribution. Note that basis functions in the \cancel{E}_T space have to be linearly independent but not necessarily orthogonal unlike the Fourier analysis.

Method For simplicity and comprehensibility, we concentrate on s -channel scalar mediator. Our method is applicable to cases of s -channel vector mediators and we summarize short proof in the Supplemental Material. We leave the study of the t -channel mediator for future work.

Basis functions used in the spectral decomposition are defined by differential cross sections, the Feynman diagram of which is given in Fig. 1 (right). In Fig. 1, VP denotes associated visible particles, and ϕ is the physical mediator whose mass is M_ϕ . In order to define basis functions, we introduce *virtual* mediators $\{\phi_i\}$ whose masses are assigned according to the invariant mass of dark matter particles, $m_{\phi_i} = m_{\chi\chi}^{(i)}$ for $i \in \{1, \dots, N\}$.

With a set of basis functions, the spectral decomposition can be understood by Fig. 1; the differential cross section of the *DM production associated with VP* [Fig. 1 (left)] is described by the linear combination of differential cross section of the *virtual mediator production* [Fig. 1 (right)]. Mathematically, it is expressed as

$$\frac{d\sigma^{\text{exp}}(X)}{dX} \simeq \sum_{i=1}^N c_i \underbrace{\left(\frac{1}{\mathcal{N}_i} \frac{d\sigma_{\phi_i}(X)}{dX} \right)}_{=\text{basis functions}}, \quad (1)$$

where X is a collider observable, e.g., \cancel{E}_T or the transverse momentum of the ISR jet. \mathcal{N}_i 's are normalization factors, $d\sigma^{\text{exp}}/dX$ is the differential cross section of physical process ($pp \rightarrow \text{VP} + \text{DM}$: Fig. 1 (left)) and $d\sigma_{\phi_i}/dX$

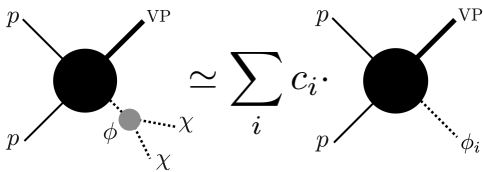


FIG. 1. A schematic diagram of the spectral decomposition of DM production.

is the differential cross section of the virtual mediator production ($pp \rightarrow VP + \phi_i$; Fig. 1 (right)). The normalization factor \mathcal{N}_i is given by

$$\mathcal{N}_i = \int_{X_{\min}}^{X_{\max}} dX \frac{d\sigma_{\phi_i}(X)}{dX}, \quad (2)$$

where $[X_{\min}, X_{\max}]$ is a range of X determined by cuts. For applying our method to data analyses, we discretize $[X_{\min}, X_{\max}]$ into $\{X_{\text{bin}}\}$.

We regard the lhs of Eq. (1) as experimental signal data after background subtraction and the rhs of (1) as the model hypothesis. Here, c_i s in Eq. (1) are fitting parameters. One can obtain $\{c_i\}$ from the standard χ^2 fitting, which minimizes

$$\chi^2 = \sum_{X_{\text{bin}}} \frac{\left(\text{Ex}(X_{\text{bin}}) - \text{SM}(X_{\text{bin}}) - \sum_{i=1}^N c_i F_i(X_{\text{bin}}) \right)^2}{\text{Ex}(X_{\text{bin}})} \quad (3)$$

where $\text{Ex}(X_{\text{bin}})$ is the experimental number of events in $X \in X_{\text{bin}}$, $\text{SM}(X_{\text{bin}})$ is obtained by the SM background calculation, and $F_i(X_{\text{bin}})$ corresponds to basis functions given by

$$F_i(X_{\text{bin}}) = \frac{L}{\mathcal{N}_i} \int_{X \in X_{\text{bin}}} dX \frac{d\sigma_{\phi_i}(X)}{dX}, \quad (4)$$

with a given integrated luminosity L . In order to obtain a unique solution from χ^2 fitting, basis functions should be linearly independent.

If X is \cancel{E}_T determined by ISR, differential distribution of X depends on a hard scale of a parton distribution function (PDF). When \cancel{E}_T is much smaller than m_{ϕ_i} , the hard scale is mostly determined by m_{ϕ_i} . In the opposite case where \cancel{E}_T is larger than m_{ϕ_i} , the hard scale is proportional to \cancel{E}_T . In other words, m_{ϕ_i} is the characteristic scale which determines the shape of corresponding basis function. In this regard, basis functions are linearly independent.

In our analyses, we have numerically confirmed linear independence by examining

$$\min_{d_j} \left[\sum_{X_{\text{bin}}} \left(N_s F_i(X_{\text{bin}}) - \sum_{j \neq i} d_j F_j(X_{\text{bin}}) \right)^2 / \text{Ex}(X_{\text{bin}}) \right] \geq \epsilon, \quad (5)$$

for all i and given total number of signal events N_s where \min_{d_j} is minimization for parameters d_j . A positive pa-

rameter ϵ is introduced to take into account statistical fluctuation. In our analyses with seven basis functions and $S/B = 1/100$, ϵ is 7.01 in 68% confidence level. A general discussion on the validity of this method can be found in Ref. [11].

In order to explicitly show the procedure, let us consider a DM model whose Lagrangian is written as

$$\mathcal{L} = \mathcal{L}_{\text{SM}} + \underbrace{\mathcal{L}_{\text{med-SM}} + \mathcal{L}_{\text{med}}}_{\rightarrow \text{basis functions}} + \underbrace{\mathcal{L}_{\text{med-DM}} + \mathcal{L}_{\text{DM}}}_{\rightarrow \text{spectral density}}, \quad (6)$$

where \mathcal{L}_{SM} is the SM Lagrangian, $\mathcal{L}_{\text{med-SM}}$ ($\mathcal{L}_{\text{med-DM}}$) is the interaction Lagrangian between the mediator and SM particles (DM particles). \mathcal{L}_{med} (\mathcal{L}_{DM}) is the kinetic term for the mediator (DM particles) including its mass. $\mathcal{L}_{\text{med-SM}} + \mathcal{L}_{\text{med}}$ affects only basis functions while $\mathcal{L}_{\text{med-DM}} + \mathcal{L}_{\text{DM}}$ governs c_i . The procedure of our method is described by following steps:

1. fix $\mathcal{L}_{\text{med-SM}} + \mathcal{L}_{\text{med}}$ and calculate basis functions,
2. obtain $\{c_i\}$ by applying Eq. (3) to the signal data,
3. find proper $\mathcal{L}_{\text{med-DM}} + \mathcal{L}_{\text{DM}}$ that matches with obtained $\{c_i\}$.

It is worth noting that one needs to specify $\mathcal{L}_{\text{med-SM}}$ in order to construct basis functions. For example, basis functions where the mediator is produced through gluon-gluon fusion is different from those where it is produced through quark and anti-quark annihilation. However, CP charge of a mediator does not affect basis functions when the mediator is s -channel. We have numerically confirmed that $\phi G_{\mu\nu} G^{\mu\nu}$ and $\phi G_{\mu\nu} \tilde{G}^{\mu\nu}$ amount to the same basis functions.¹ The mediator models (*i.e.*, $\mathcal{L}_{\text{med-DM}}$) can be inferred by other collider variables such as an angular correlation between jets in $jj + \cancel{E}_T$ channel [12]. It is also possible to concentrate on the test of mediator itself by using a visible decay mode and checking its consistency [13].

Spectral density The physical meaning of c_i is the DM invariant mass ($m_{\chi\chi}$) distribution,

$$c_i \simeq \frac{d\sigma^{\text{exp}}(m_{\chi\chi}^{(i)})}{dm_{\chi\chi}} \Delta m_{\chi\chi}^{(i)}. \quad (7)$$

where $\Delta m_{\chi\chi}^{(i)} = (m_{\chi\chi}^{(i+1)} - m_{\chi\chi}^{(i-1)})/2$. c_i is related to the Källén-Lehmann spectral density $\rho_{\phi \rightarrow \chi\chi}(m_{\chi\chi}^{(i)}, M_\phi)$ [14] by

$$c_i = 2m_{\chi\chi}^{(i)} \Delta m_{\chi\chi}^{(i)} \mathcal{N}_i \rho_{\phi \rightarrow \chi\chi}(m_{\chi\chi}^{(i)}, M_\phi). \quad (8)$$

¹ For other interactions, it can be inferred from Ref. [9].

The spectral density $\rho_{\phi \rightarrow \chi\chi}(m_{\chi\chi}^{(i)}, M_\phi)$ is given by

$$\rho_{\phi \rightarrow \chi\chi}(m_{\chi\chi}^{(i)}, M_\phi) = \frac{1}{\pi} |G_\phi(m_{\chi\chi}^{(i)}, M_\phi)|^2 m_{\chi\chi}^{(i)} \Gamma_{\phi_i \rightarrow \chi\chi}(m_{\chi\chi}^{(i)}), \quad (9)$$

where $G_\phi(m_{\chi\chi}^{(i)}, M_\phi)$ is the propagator of ϕ with energy transfer $m_{\chi\chi}^{(i)}$ and on-shell mass M_ϕ and $\Gamma_{\phi_i \rightarrow \chi\chi}(m_{\chi\chi}^{(i)})$ is the decay rate of process $\phi_i \rightarrow \chi\chi$ with mass $m_{\phi_i} = m_{\chi\chi}$. $\rho_{\phi \rightarrow \chi\chi}(m_{\chi\chi}^{(i)}, M_\phi)$ does not depend on collider observables, X (e.g. p_T , rapidity or \cancel{E}_T , etc.) or cut variables. In addition, it is independent of channels (e.g. mono-jet, mono- Z , etc.) and collider energy. This feature guarantees that the spectral decomposition is valid up to detector level. Mathematical proofs are given in the Supplemental Material and its numerical validation is given in the next section.

Although basis functions depend on mediator models, the spectral decomposition method make analyses less model dependent. Once we specify $\mathcal{L}_{\text{med-SM}} + \mathcal{L}_{\text{med}}$ (step 1), we can obtain spectral density from the signal data (step 2) and infer $\mathcal{L}_{\text{med-DM}} + \mathcal{L}_{\text{DM}}$ through physical insights (step 3).

Here, we discuss some possible cases for the connection between spectral densities and the DM interactions in $\mathcal{L}_{\text{med-DM}} + \mathcal{L}_{\text{DM}}$. When a mediator ϕ is heavier than DM threshold ($M_\phi > 2m_\chi$), $\rho_{\phi \rightarrow \chi\chi}$ will be described by the Breit-Wigner distribution. In the case of $M_\phi < 2m_\chi$, $\rho_{\phi \rightarrow \chi\chi}$ will be proportional to the power of DM's velocity v_χ , $\rho_{\phi \rightarrow \chi\chi} \propto v_\chi^{2J_0+1}$. If $m_\chi < M_\phi < 2m_\chi$ and the dominant annihilation can be $\chi\chi \rightarrow \text{SM}$ particles through the mediator,² it may be possible to infer the velocity dependence of DM annihilation process at the thermal freeze-out due to the time reversal symmetry [6],

$$\langle \sigma_{\text{ann}} v_\chi \rangle \equiv \sigma_0 v_\chi^{2J_0} + \mathcal{O}(v_\chi^{2J_0+2}), \quad (10)$$

where it corresponds to s -wave (p -wave) if $J_0 = 0$ (1). Some nontrivial spectral densities can be obtained when non-renormalizable operators [8] or resonance spectrum ($M_\phi \simeq 2m_\chi$) [15] are considered.

Compared to previous studies relying on Monte Carlo simulations, the spectral decomposition becomes more powerful when the dark sector is complicated. For example, if there exist several DM species (heavier than M_ϕ), $m_{\chi\chi}$ distribution from the spectral decomposition has multi-threshold behavior. At each threshold, we can count the power of v_χ in order to identify the interaction. For another example, let us consider the production of two mediator particles; the one is on-shell ($M_{\phi_1} > 2m_\chi$) and the other is off-shell ($M_{\phi_2} < 2m_\chi$). Our procedure will recover the Breit-Wigner resonance of $\phi_1 \rightarrow \chi\chi$ process, standing on the middle of continuum distribution

from $\phi_2 \rightarrow \chi\chi$. Such a situation can be realized in various Higgs portal models, where both Higgs boson and singlet scalar produce DM particles through mixing. In addition, the spectral decomposition can be used to vary whether or not DM particles form a bound state. A bound state resonance will be located slightly below the DM threshold at $m_{\chi\chi}$ distribution. The theoretical prediction is obtained by solving non-relativistic Schrödinger equation [16], and thus we may be able to see the trace of Sommerfeld enhancement in the dark matter annihilation process [17].

LHC Example. In order to show the detail, we provide a specific example where we set the center of mass energy to be 14 TeV and the integrated luminosity to be 3 ab^{-1} .

Step 1. Our toy model includes a real scalar mediator ϕ which interacts with SM through the dimension 5 operator, $\phi G^{\mu\nu} G_{\mu\nu}$. We consider $X = \cancel{E}_T$ distribution of the mono-jet process ($pp \rightarrow j\chi\chi$). Once we fix $\mathcal{L}_{\text{med-SM}} + \mathcal{L}_{\text{med}}$, we can calculate basis functions (i.e., differential cross section of ($pp \rightarrow j\phi_i$)) with a given set of $\{m_{\chi\chi}^{(i)}\}$. In this example, we set $\{m_{\chi\chi}^{(i)}\} = \{10, 200, 400, 700, 1100, 2000, 5000\}$ in GeV units. We take a larger gap between $m_{\chi\chi}^{(i)}$'s at higher $m_{\chi\chi}^{(i)}$ so that basis functions are distinguishable in \cancel{E}_T space. For numerical analyses, a number of tools are used; FeynRules 2.0/MadGraph_aMC@NLO [18] for parton level event generation, Pythia 8.1 [19] for parton showering/hadronization and Delphes 3 [20]/Fastjet 3 [21] for detector level event reconstruction with ATLAS detector delphes card. Jets are reconstructed by the anti- k_T algorithm with jet radius parameter 0.4. We select events with $\cancel{E}_T > 200$ GeV and at least one jet having $p_T^j > 100$ GeV and $|\eta^j| < 2.5$. We choose \cancel{E}_T bin size to be 10% of \cancel{E}_T , which corresponds to p_T resolution of the jet at the LHC [22] and the range of \cancel{E}_T is taken from 200 GeV to 2 TeV.

Step 2. We decompose signal distributions into basis functions according to Eq.(1) with $X = \cancel{E}_T$. We generate signal distributions from pseudo-experiments (PEs). We choose scalar dark matter (trilinear interaction with the mediator: s -wave) and fermionic dark matter (Yukawa interaction with the mediator: p -wave) for signal distributions. A DM mass is set to be $m_\chi = 200$ GeV, so the threshold is at $2m_\chi = 400$ GeV. In the Fig. 2, their \cancel{E}_T distributions are shown as black dotted lines on the top of each plot.

By following the fitting procedure explained in previous sections, we decompose signal distributions into basis functions. In the Fig. 2, it is illustrated that basis functions (shaded by different colors) are piled into the overall distribution (black dotted line). The area of each basis function in Fig. 2 is equal to a normalized coefficient,

$$\hat{c}_i = c_i / \sum c_i. \quad (11)$$

² For $m_\chi > m_\phi$ case, the dominant process can be $\chi\chi \rightarrow \phi\phi$.

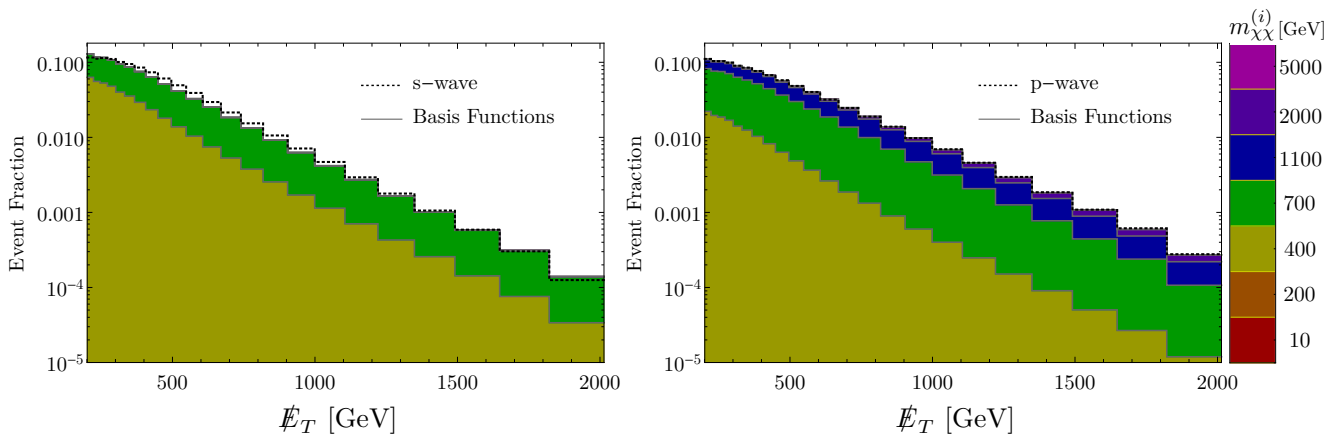


FIG. 2. Missing transverse energy (\cancel{E}_T) distribution of mono-jet process in toy model. Black dotted lines correspond to the signal distributions of s -wave (left) and p -wave (right) processes. Dark matter mass is set to be 200 GeV. Signal distributions are decomposed into basis functions (colored) whose different colors represent the value of $m_{\chi\chi}^{(i)}$, as in the bar on the right.

which corresponds to DM invariant mass distribution. Different colors indicate different $m_{\chi\chi}^{(i)}$ s whose corresponding numbers are shown in the bar on the right-hand side. By comparing the areas of two panels in Fig. 2, we can see that the s -wave process (left) tends to be more distributed around the DM threshold ($m_{\chi\chi} = 400$ GeV) than the p -wave process (right).

Step 3 Coefficients $\{\hat{c}_i\}$ show the DM invariant mass distribution from which we can infer the interaction between the mediator and DM particles. In Fig. 3, we show four cases of the 200 GeV DM production in $m_{\chi\chi}$ are plotted; invisible decay of the on-shell mediator (red), s -wave through the off-shell mediator (green), p -wave through the off-shell mediator (blue) and s -wave through the off-shell mediator with a DM bound state near threshold (dark green dashed). While the true values of \hat{c}_i s are shown in the left panel, \hat{c}_i s obtained by our method are shown in the middle (right) panel for signal-to-background ratio $S/B = 1/100$ ($1/250$). On-shell production of the mediator (red) causes only one bin to be non-zero among $m_{\chi\chi}^{(i)}$ s due to the Breit-Wigner resonance ($m_{\chi\chi} = M_\phi = 700$ GeV). For off-shell cases, coefficients are non-zero in a broad range of $m_{\chi\chi}^{(i)}$ and the first non-zero bin corresponds to the threshold, $2m_\chi = 400$ GeV. In the case of the s -wave process (green), events are more distributed near the threshold than those in the case of p -wave process (blue) because of v_χ dependence. If there exists a bound state resonance (dark green dashed) it makes a larger value in the first nonzero bin.³ In middle and right panels, statistical errors are denoted by shaded

bands (except for bound state case) and their discrimination power can be estimated. While lines are separated enough to be distinguished for $S/B = 1/100$, there are relatively large overlap in error bands for $S/B = 1/250$. Significances for $S/B = 1/250$ are summarized in Table. I.

We estimate errors in fitting c_i s by the following procedure. We take the SM background of $pp \rightarrow j + Z$ ($Z \rightarrow \nu\bar{\nu}$) parton level process. A more precise SM estimation can be found in Ref. [23] which also includes $pp \rightarrow j + W$ ($W \rightarrow l\nu$) and other processes. To make the expected number of events consistent with Ref. [23], we multiply the energy dependent K -factor $\text{Max}(1, -\cancel{E}_T/(400 \text{ GeV}) + 2.6)$. The total number of signal events is fixed by setting $S/B = 1/250$ and $1/100$. For each \cancel{E}_T bin, we generate 10^4 of pseudoexperiments (PE) by a Poissonian random number generator. Then the fitting procedure is repeated to obtain 10^4 different sets of $\{\hat{c}_i^{(\text{PE})}\}$ for each PE. From them, we obtain probability density distribution of $\{\hat{c}_i\}$ and estimate the expected value of $\{\hat{c}_i\}$ (solid lines) and expected 68% errors (shaded bands).

From this example, we notice that a large number of signal events are required to identify the dark sector. In Fig. 3, the corresponding S/\sqrt{B} 's are 8 (middle) and 3 (right) for 30 fb^{-1} at 13 TeV, which are almost excluded at current LHC searches. Nevertheless, even for $S/B = 1/250$ benchmark point, some cases in Fig. 3 are distinguishable and we summarize the corresponding significance in Table I.

The resolution of $m_{\chi\chi}$ (i.e., how small bins can be) can be regarded as the distinguishability of basis functions (i.e., how large ϵ in Eq. (5) is). While the distinguishability is mostly affected by the statistical fluctuation in our analyses, a real analysis must take into account systematic uncertainties in the calculation of basis functions. In

³ Here, the bound state resonance cross section is set to be 15% of the total cross section. Such a case corresponds to $g_{\text{DM}}^2/(4\pi) \simeq 0.35$ (g_{DM} : gauge coupling constant in the dark sector) if DM particle is in $\text{SU}(3)_{\text{DM}}$ fundamental representation.

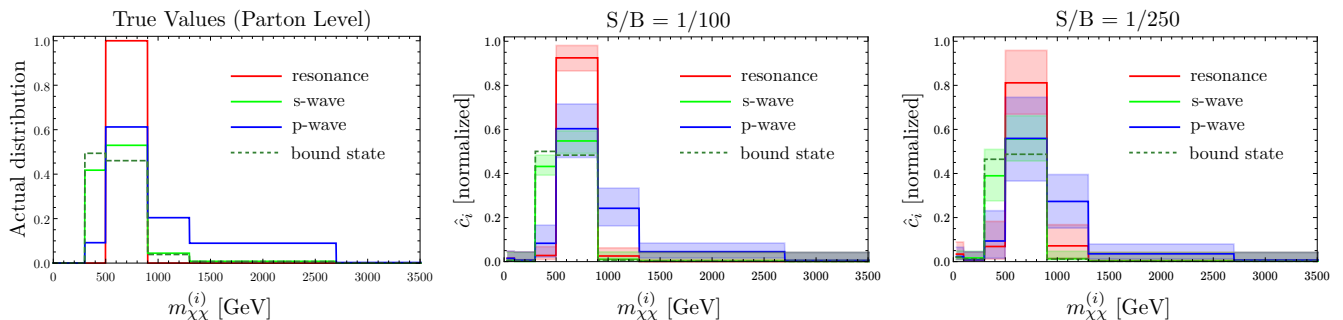


FIG. 3. DM invariant mass ($m_{\chi\chi}$) distribution for DM mass $m_\chi = 200$ GeV, center of mass energy 14 TeV and integrated luminosity $L = 3 \text{ ab}^{-1}$. We consider four cases: DM particles are produced in resonance decay of the ϕ at 700 GeV (red), in the continuum in the s -wave (green), in the continuum in the p -wave (blue) and in the continuum in the s -wave with bound state near threshold. For the resonance case, $M_\phi = 700 \text{ GeV} > 2m_\chi$ while for other cases, $M_\phi = 30 \text{ GeV}$. Their true distributions are given in the left panel. In right two panels, $\{\hat{c}_i\}$ obtained by our method are plotted with signal to background ratio $S/B = 1/100$ (middle) and $1/250$ (right).

signal \ hypothesis	resonance	s -wave	p -wave	bound st.
resonance		1.62σ	2.22σ	2.15σ
s -wave	4.30σ		4.20σ	0.943σ
p -wave	1.68σ	2.21σ		2.90σ
bound st.	4.48σ	1.33σ	4.45σ	

TABLE I. Expected significance when the signal distribution given in the first column is fitted by hypothesis given in the first row. Signal number of events is fixed by $S/B = 1/250$ with 3 ab^{-1} at 14 TeV.

order to precisely estimate systematic uncertainties, full detector simulations with the best tools are required.

Conclusion and discussion. The spectral decomposition allows us to extract DM invariant mass distribution even at hadron colliders. When DM particles are produced via s -channel mediators, basis functions of the spectral decomposition do not depend on DM properties, while coefficients $\{c_i\}$ (or $\rho_{\chi \rightarrow \chi\chi}$) contain detailed information of dark matter particles.

One of the most challenging issues in our approach is the requirement of a large number of signal events to identify the dark sector at hadron colliders. Until now, the LHC has no signal excess of DM in all the mono-X channels: mono-jet [23], mono-photon, [24], mono-Z [25] and mono-Higgs [26]. The integrated luminosity is, now, about 30 fb^{-1} . This means that if we set $S/\sqrt{B} < 2$ at $L = 30 \text{ fb}^{-1}$, then it will become, at most, $S/\sqrt{B} < 20$ at the end of projected high luminosity (HL) run of $L = 3 \text{ ab}^{-1}$. Nevertheless, it can be resolved if we combine signal data of various channels together with collider observables other than \cancel{E}_T . In addition, in the next-generation collider (e.g., 100 TeV proton-proton collider), better S/B can be achieved in DM signals, so the spectral decomposition is useful to understand the dark sector.

Acknowledgements. This work is supported by the institute for basic science under the project code, IBS-

R018-D1.

* kyujungbae@ibs.re.kr

† thjung0720@ibs.re.kr

‡ parc.seoultech@seoultech.ac.kr

- [1] B. W. Lee and S. Weinberg, Phys. Rev. Lett. **39**, 165 (1977). doi:10.1103/PhysRevLett.39.165
- [2] G. Jungman, M. Kamionkowski and K. Griest, Phys. Rept. **267**, 195 (1996) [hep-ph/9506380]. G. Bertone, D. Hooper and J. Silk, Phys. Rept. **405**, 279 (2005) [hep-ph/0404175].
- [3] A. Tan *et al.* [PandaX-II Collaboration], Phys. Rev. Lett. **117**, no. 12, 121303 (2016) [arXiv:1607.07400 [hep-ex]]; D. S. Akerib *et al.*, arXiv:1608.07648 [astro-ph.CO]. D. S. Akerib *et al.* [LUX Collaboration], Phys. Rev. Lett. **118** (2017) no.2, 021303. C. Amole *et al.* [PICO Collaboration], arXiv:1702.07666 [astro-ph.CO].
- [4] M. L. Ahnen *et al.* [MAGIC and Fermi-LAT Collaborations], JCAP **1602** (2016) no.02, 039.
- [5] W. Frazer, *Elementary Particles*, Prentice-Hall (1966)
- [6] A. Birkedal, K. Matchev and M. Perelstein, Phys. Rev. D **70**, 077701 (2004) doi:10.1103/PhysRevD.70.077701 [hep-ph/0403004]. J. L. Feng, S. Su and F. Takayama, Phys. Rev. Lett. **96**, 151802 (2006) doi:10.1103/PhysRevLett.96.151802 [hep-ph/0503117]. P. Konar, K. Kong, K. T. Matchev and M. Perelstein, New J. Phys. **11**, 105004 (2009) doi:10.1088/1367-2630/11/10/105004 [arXiv:0902.2000 [hep-ph]].
- [7] C. Bartels, O. Kittel, U. Langenfeld and J. List, arXiv:1202.6516 [hep-ex]. S. Y. Choi, T. Han, J. Kalinowski, K. Rolbiecki and X. Wang, Phys. Rev. D **92**, no. 9, 095006 (2015) doi:10.1103/PhysRevD.92.095006 [arXiv:1503.08538 [hep-ph]]. T. Kamon, P. Ko and J. Li, arXiv:1705.02149 [hep-ph].
- [8] D. Barducci *et al.*, JHEP **1701**, 078 (2017) doi:10.1007/JHEP01(2017)078 [arXiv:1609.07490 [hep-ph]].
- [9] A. Belyaev, L. Panizzi, A. Pukhov and M. Thomas, JHEP **1704**, 110 (2017) doi:10.1007/JHEP04(2017)110 [arXiv:1610.07545 [hep-ph]].

- [10] C. F. Uhlemann and N. Kauer, Nucl. Phys. B **814**, 195 (2009) doi:10.1016/j.nuclphysb.2009.01.022 [arXiv:0807.4112 [hep-ph]].
- [11] T. H. Jung and M. Park, in preparation.
- [12] M. R. Buckley, B. Heinemann, W. Klemm and H. Murayama, Phys. Rev. D **77**, 113017 (2008) doi:10.1103/PhysRevD.77.113017 [arXiv:0804.0476 [hep-ph]]. K. Hagiwara, Q. Li and K. Mawatari, JHEP **0907**, 101 (2009) doi:10.1088/1126-6708/2009/07/101 [arXiv:0905.4314 [hep-ph]]. M. R. Buckley and M. J. Ramsey-Musolf, JHEP **1109**, 094 (2011) doi:10.1007/JHEP09(2011)094 [arXiv:1008.5151 [hep-ph]].
- [13] The ATLAS collaboration [ATLAS Collaboration], Summary plots from the ATLAS Exotic physics group (2017). CMS Collaboration [CMS Collaboration], Dark Matter Summary Plots from CMS for LHCP 2017. [14]
- [14] M. E. Peskin and D. V. Schroeder, Reading, USA: Addison-Wesley (1995) 842 p
- [15] D. Chway, T. H. Jung and H. D. Kim, J. Korean Phys. Soc. **69**, no. 1, 16 (2016) doi:10.3938/jkps.69.16 [arXiv:1502.03541 [hep-ph]].
- [16] M. J. Strassler and M. E. Peskin, Phys. Rev. D **43**, 1500 (1991). doi:10.1103/PhysRevD.43.1500
- [17] A. Sommerfeld, Annalen der Physik 403, 257 (1931). J. Hisano, S. Matsumoto, M. M. Nojiri and O. Saito, Phys. Rev. D **71**, 063528 (2005) doi:10.1103/PhysRevD.71.063528 [hep-ph/0412403]. N. Arkani-Hamed, D. P. Finkbeiner, T. R. Slatyer and N. Weiner, Phys. Rev. D **79**, 015014 (2009) doi:10.1103/PhysRevD.79.015014 [arXiv:0810.0713 [hep-ph]].
- [18] A. Alloul, N. D. Christensen, C. Degrande, C. Duhr and B. Fuks, Comput. Phys. Commun. **185**, 2250 (2014) doi:10.1016/j.cpc.2014.04.012 [arXiv:1310.1921 [hep-ph]]. J. Alwall *et al.*, JHEP **1407**, 079 (2014) doi:10.1007/JHEP07(2014)079 [arXiv:1405.0301 [hep-ph]].
- [19] T. Sjostrand, S. Mrenna and P. Z. Skands, Comput. Phys. Commun. **178**, 852 (2008) doi:10.1016/j.cpc.2008.01.036 [arXiv:0710.3820 [hep-ph]].
- [20] J. de Favereau *et al.* [DELPHES 3 Collaboration], JHEP **1402**, 057 (2014) doi:10.1007/JHEP02(2014)057 [arXiv:1307.6346 [hep-ex]].
- [21] M. Cacciari and G. P. Salam, Phys. Lett. B **641**, 57 (2006) doi:10.1016/j.physletb.2006.08.037 [hep-ph/0512210]. M. Cacciari, G. P. Salam and G. Soyez, Eur. Phys. J. C **72**, 1896 (2012) doi:10.1140/epjc/s10052-012-1896-2 [arXiv:1111.6097 [hep-ph]].
- [22] V. Khachatryan *et al.* [CMS Collaboration], JINST **12**, no. 02, P02014 (2017) doi:10.1088/1748-0221/12/02/P02014 [arXiv:1607.03663 [hep-ex]].
- [23] M. Aaboud *et al.* [ATLAS Collaboration], Phys. Rev. D **94**, no. 3, 032005 (2016) doi:10.1103/PhysRevD.94.032005 [arXiv:1604.07773 [hep-ex]]. CMS Collaboration [CMS Collaboration], CMS-PAS-EXO-16-048.
- [24] M. Aaboud *et al.* [ATLAS Collaboration], arXiv:1704.03848 [hep-ex]. CMS Collaboration [CMS Collaboration], CMS-PAS-EXO-16-039.
- [25] The ATLAS collaboration [ATLAS Collaboration], ATLAS-CONF-2016-056. CMS Collaboration [CMS Collaboration], CMS-PAS-EXO-16-052.
- [26] The ATLAS collaboration, ATLAS-CONF-2016-019. CMS Collaboration [CMS Collaboration], CMS-PAS-EXO-16-054.

SUPPLEMENTAL MATERIAL: PROOFS OF SPECTRAL DECOMPOSITION

Derivation of spectral decomposition

We begin with scalar mediator and we will extend the proof to the case where dark matter particle has a vector coupling with massive vector boson (see Sec. “vector mediator”). We consider a process $A + B \rightarrow VP + \chi\chi$ where A and B denote initial partons. VP stands for “visibls particles” (e.g. jet, photon, lepton). For s -channel scalar mediator models, the scattering amplitude of $(A + B \rightarrow VP + \chi\chi)$ is factorized as

$$\mathcal{M}_{\text{signal}} = \mathcal{M}_{A+B \rightarrow VP+\phi} G_{\phi}(m_{\chi\chi}, M_{\phi}) \mathcal{M}_{\phi \rightarrow \chi\chi}, \quad (12)$$

where $\mathcal{M}_{A+B \rightarrow VP+\phi}$ is the amplitude of production part ($A + B \rightarrow VP + \phi$), ϕ is a virtual mediator, $\mathcal{M}_{\phi \rightarrow \chi\chi}$ is amplitude of decaying part ($\phi \rightarrow \chi\chi$) and $G_{\phi}(m_{\chi\chi}, M_{\phi})$ is the propagator of virtual mediator with a momentum transfer $m_{\chi\chi}$ and on-shell mass M_{ϕ} . By using the factorization of the amplitude, the signal cross section of $(A + B \rightarrow VP + \chi\chi)$ can be expressed by,

$$\hat{\sigma}_{\text{signal}} = \frac{1}{2s} \int d\Phi_{VP} d\Phi_{DM} |\mathcal{M}_{A+B \rightarrow VP+\phi}|^2 |G_{\phi}(p_{\phi}, M_{\phi})|^2 |\mathcal{M}_{\phi \rightarrow \chi\chi}|^2 (2\pi)^4 \delta^{(4)}\left(\sum_{i \in \text{ext}} p_i\right), \quad (13)$$

where $d\Phi_{VP} = \prod_{i \in VP} \frac{d^3 \vec{p}_i}{2E_i (2\pi)^3}$, $d\Phi_{DM} = \prod_{i \in DM} \frac{d^3 \vec{p}_i}{2E_i (2\pi)^3}$. We denote $\hat{\sigma}$ (σ) by cross section calculated before (after) parton distribution function (PDF) convolution. By inserting identity,

$$1 = \int dp_{\phi}^0 \frac{d^3 \vec{p}_{\phi}}{(2\pi)^3} (2\pi)^3 \delta^{(4)}(p_{\phi} - \sum_{i \in DM} p_i) = \int dm_{\chi\chi}^2 d\Phi_{\phi} (2\pi)^4 \delta^{(4)}(p_{\phi} - \sum_{i \in DM} p_i), \quad (14)$$

with $m_{\chi\chi}^2 = p_\phi^0{}^2 - |\vec{p}_\phi|^2$ and $d\Phi_\phi(m_{\chi\chi}) = \frac{d^3\vec{p}_\phi}{2p_\phi^0(2\pi)^3}$, we obtain

$$\hat{\sigma}_{\text{signal}} = \int dm_{\chi\chi}^2 \frac{1}{2s} \int d\Phi_{\text{VP}} d\Phi_\phi |\mathcal{M}_{A+B \rightarrow \text{VP}+\phi}|^2 (2\pi)^4 \delta^{(4)}\left(\sum_{i \in \text{ext}} p_i\right) \quad (15)$$

$$\times |G_\phi(m_{\chi\chi}, M_\phi)|^2 \frac{1}{2\pi} \int d\Phi_{\text{DM}} |\mathcal{M}_{\phi \rightarrow \chi\chi}|^2 (2\pi)^4 \delta^{(4)}\left(p_\phi - \sum_{i \in \text{DM}} p_i\right) \quad (16)$$

$$= \int dm_{\chi\chi}^2 \hat{\sigma}_{A+B \rightarrow \text{VP}+\phi}(m_{\chi\chi}) \cdot \rho_{\phi \rightarrow \chi\chi}(m_{\chi\chi}, M_\phi), \quad (17)$$

where $\hat{\sigma}_{A+B \rightarrow \text{VP}+\phi}(m_{\chi\chi})$ denotes the (virtual) mediator production cross section and $\rho_{\phi \rightarrow \chi\chi}(m_{\chi\chi}, M_\phi)$ is a spectral density, *i.e.*,

$$\hat{\sigma}_{A+B \rightarrow \text{VP}+\phi}(m_{\chi\chi}) = \frac{1}{2s} \int d\Phi_{\text{VP}} d\Phi_\phi |\mathcal{M}_{A+B \rightarrow \text{VP}+\phi}|^2 (2\pi)^4 \delta^{(4)}\left(\sum_{i \in \text{ext}} p_i\right), \quad (18)$$

$$\rho_{\phi \rightarrow \chi\chi}(m_{\chi\chi}, M_\phi) = |G_\phi(m_{\chi\chi}, M_\phi)|^2 \frac{1}{2\pi} \int d\Phi_{\text{DM}} |\mathcal{M}_{\phi \rightarrow \chi\chi}|^2 (2\pi)^4 \delta^{(4)}\left(p_\phi - \sum_{i \in \text{DM}} p_i\right), \quad (19)$$

where mass of ϕ equals to the integral variable $m_{\chi\chi}$. In Eq. (17), phase space information of visible particles is encoded solely inside $\hat{\sigma}_{A+B \rightarrow \text{VP}+\phi}(m_{\chi\chi})$. It is noteworthy that spectral density, $\rho_{\phi \rightarrow \chi\chi}(m_{\chi\chi}, M_\phi)$ defined in (19) does not depend on information of visible particles (*i.e.*, incoming momenta of partons and outgoing momenta of VP). This feature plays a crucial role in following arguments.

We take a derivative of Eq. (17), d/dX (X : any function of visible particles' momenta, *e.g.*, \cancel{E}_T , H_T , $p_T^{(j_1)}$, *etc.*),

$$\frac{d\hat{\sigma}_{\text{signal}}(X)}{dX} = \int dm_{\chi\chi}^2 \frac{d\hat{\sigma}_{A+B \rightarrow \text{VP}+\phi}(m_{\chi\chi}, X)}{dX} \cdot \rho_{\phi \rightarrow \chi\chi}(m_{\chi\chi}, M_\phi). \quad (20)$$

The differential operator d/dX only acts on $\hat{\sigma}_{A+B \rightarrow \text{VP}+\phi}$. Eq. (21) holds after PDF convolution, *i.e.*,

$$\frac{d\sigma_{\text{signal}}(X)}{dX} = \int dm_{\chi\chi}^2 \frac{d\sigma_{pp \rightarrow \text{VP}+\phi}(m_{\chi\chi}, X)}{dX} \cdot \rho_{\phi \rightarrow \chi\chi}(m_{\chi\chi}, M_\phi). \quad (21)$$

Detector level

The spectral decomposition is applicable to detector level. Let us consider a function F which transfers the parton level distribution to the detector level distribution,

$$F : \text{parton level distribution} \rightarrow \text{detector level distribution} \quad (22)$$

$$\frac{d\sigma_{\text{signal}}(k_1, k_2, \dots, k_m)}{dk_1 dk_2 \dots dk_m} \rightarrow F\left(\frac{d\sigma_{\text{signal}}(q_1, q_2, \dots, q_n)}{dq_1 dq_2 \dots dq_n}\right), \quad (23)$$

where k_i 's denote momenta of visible particles at parton level and q_i 's denote momenta of final particles at detector level. If we insert Eq. (21) into $F\left(\frac{d\sigma_{\text{signal}}}{dk_1 dk_2 \dots dk_m}\right)$, then we obtain

$$F\left(\frac{d\sigma_{\text{signal}}(X)}{dX}\right) = \int dm_{\chi\chi}^2 F\left(\frac{d\sigma_{pp \rightarrow \text{VP}+\phi}(m_{\chi\chi}, X)}{dX}\right) \cdot \rho_{\phi \rightarrow \chi\chi}(m_{\chi\chi}, M_\phi), \quad (24)$$

since $\rho_{\phi \rightarrow \chi\chi}$ does not depend on k_i 's. Here, F should include parton showering, hadronization, jet clustering algorithm, detector smearing effects and detector efficiency.

Meaning of coefficients

For each $m_{\chi\chi}$, we define the normalization function

$$\mathcal{N}(m_{\chi\chi}) = \int_{X=X_{\min}}^{X_{\max}} dX \frac{d\sigma_{pp \rightarrow VP+\phi}(m_{\chi\chi}, X)}{dX}. \quad (25)$$

From Eq. (21) and Eq. (25), we obtain

$$\frac{d\sigma_{\text{signal}}(X)}{dX} = \int dm_{\chi\chi}^2 \mathcal{N}(m_{\chi\chi}) \rho_{\phi \rightarrow \chi\chi}(m_{\chi\chi}, M_\phi) \left(\frac{1}{\mathcal{N}(m_{\chi\chi})} \frac{d\sigma_{pp \rightarrow VP+\phi}(m_{\chi\chi}, X)}{dX} \right) \quad (26)$$

$$= \int dm_{\chi\chi} 2m_{\chi\chi} \mathcal{N}(m_{\chi\chi}) \rho_{\phi \rightarrow \chi\chi}(m_{\chi\chi}, M_\phi) \left(\frac{1}{\mathcal{N}(m_{\chi\chi})} \frac{d\sigma_{pp \rightarrow VP+\phi}(m_{\chi\chi}, X)}{dX} \right). \quad (27)$$

We change integral variable $m_{\chi\chi}$ into a discrete set $\{m_{\chi\chi}^{(1)}, m_{\chi\chi}^{(2)}, \dots, m_{\chi\chi}^{(N)}\}$. All functions of $m_{\chi\chi}$ become series with sub-index i (e.g. $\mathcal{N}(m_{\chi\chi}^{(i)}) = \mathcal{N}_i$). We denote $d\sigma_{pp \rightarrow VP+\phi}(m_{\chi\chi}^{(i)}, X) = d\sigma_{\phi_i}(X)$. Finally, we obtain Eq. (1) in the manuscript,

$$\frac{d\sigma_{\text{signal}}(X)}{dX} \simeq \sum_{i=1}^N c_i \underbrace{\left(\frac{1}{\mathcal{N}_i} \frac{d\sigma_{\phi_i}(X)}{dX} \right)}_{=\text{basis functions}}, \quad (28)$$

with Eq. (8) in the manuscript,

$$c_i = 2m_{\chi\chi}^{(i)} \Delta m_{\chi\chi}^{(i)} \mathcal{N}_i \rho_{\phi \rightarrow \chi\chi}(m_{\chi\chi}^{(i)}, M_\phi). \quad (29)$$

On the other hand, from the Eq. (21), the $m_{\chi\chi}$ distribution is given by

$$\frac{d\sigma_{\text{signal}}(m_{\chi\chi})}{dm_{\chi\chi}} = \int_{X=X_{\min}}^{X_{\max}} dX \frac{d\sigma_{\text{signal}}(X)}{dm_{\chi\chi} dX} = \int_{X=X_{\min}}^{X_{\max}} dX 2m_{\chi\chi} \frac{d\sigma_{pp \rightarrow VP+\phi}(m_{\chi\chi}, X)}{dX} \cdot \rho_{\phi \rightarrow \chi\chi}(m_{\chi\chi}, M_\phi) \quad (30)$$

$$= 2m_{\chi\chi} \mathcal{N}(m_{\chi\chi}) \rho_{\phi \rightarrow \chi\chi}(m_{\chi\chi}, M_\phi) = c_i / \Delta m_{\chi\chi}^{(i)}. \quad (31)$$

It proves Eq. (7) in the manuscript,

$$\frac{d\sigma_{\text{signal}}(m_{\chi\chi}^{(i)})}{dm_{\chi\chi}} \Delta m_{\chi\chi}^{(i)} \simeq c_i. \quad (32)$$

Vector mediator

In this section, we show spectral decomposition for the vector mediator case. In the unitary gauge, the tree-level propagator of the massive vector boson is given by

$$\begin{aligned} G_\phi^{(\text{tree})}(k, M_\phi)^{\mu\nu} &= \frac{-i}{k^2 - M_\phi^2} \left(g^{\mu\nu} - \frac{k^\mu k^\nu}{M_\phi^2} \right) \\ &= \frac{-i}{k^2 - M_\phi^2} \left(g^{\mu\nu} - \frac{k^\mu k^\nu}{k^2} \right) - \frac{-i}{M_\phi^2} \frac{k^\mu k^\nu}{k^2} \end{aligned} \quad (33)$$

where we separate the propagator into the transverse part ($g^{\mu\nu} - k^\mu k^\nu / k^2$) and the longitudinal part ($k^\mu k^\nu / k^2$). This form is convenient to resum vacuum polarization tensor $\Pi_{\mu\nu}$ when the spectral decomposition is applied to all orders of perturbation theory. The vacuum polarization tensor is also split into transverse and longitudinal parts,

$$-i\Pi_{\mu\nu} = \left(-g_{\mu\nu} + \frac{k_\mu k_\nu}{k^2} \right) \Pi_T + \frac{k_\mu k_\nu}{k^2} \Pi_L. \quad (34)$$

After resummation of vacuum polarization, we obtain the propagator,

$$G_\phi^{\mu\nu} = G_\phi^{(\text{tree})\mu\nu} + G_\phi^{(\text{tree})\mu\rho_1} \Pi_{\rho_1\sigma_1} G_\phi^{(\text{tree})\sigma_1\nu} + \dots \quad (35)$$

$$= \frac{1}{k^2 - M_\phi^2} \left(g^{\mu\nu} - \frac{k^\mu k^\nu}{k^2} \right) \left(1 + \frac{1}{k^2 - M_\phi^2} \Pi_T + \left(\frac{1}{k^2 - M_\phi^2} \Pi_T \right)^2 + \dots \right) \quad (36)$$

$$+ \frac{1}{M_\phi^2} \frac{k^\mu k^\nu}{k^2} \left(1 + \frac{1}{M_\phi^2} \Pi_L + \left(\frac{1}{M_\phi^2} \Pi_L \right)^2 + \dots \right) \quad (37)$$

$$= G_T(k^2, M_\phi^2) \left(g_{\mu\nu} - \frac{k_\mu k_\nu}{k^2} \right) - G_L(k^2, M_\phi^2) \frac{k_\mu k_\nu}{k^2} \quad (38)$$

where $G_T = -i/(k^2 - M_\phi^2 - \Pi_T)$ and $G_L = i/(M_\phi^2 + \Pi_L)$.

Based on above treatment of vector propagator, the scattering amplitude of $(A + B \rightarrow \text{VP} + \chi\chi)$ becomes

$$\mathcal{M}_{\text{signal}} = \mathcal{M}_{A+B \rightarrow \text{VP}+\phi}^\mu G_\phi(m_{\chi\chi}, M_\phi)_{\mu\nu} \mathcal{M}_{\phi \rightarrow \chi\chi}^\nu, \quad (39)$$

$$= \underbrace{\mathcal{M}_{A+B \rightarrow \text{VP}+\phi}^\mu G_T(m_{\chi\chi}, M_\phi) \left(g_{\mu\nu} - \frac{k_\mu k_\nu}{k^2} \right) \mathcal{M}_{\phi \rightarrow \chi\chi}^\nu}_{=\text{transverse part}} + \underbrace{\mathcal{M}_{A+B \rightarrow \text{VP}+\phi}^\mu G_L(m_{\chi\chi}, M_\phi) \frac{k_\mu k_\nu}{k^2} \mathcal{M}_{\phi \rightarrow \chi\chi}^\nu}_{\text{longitudinal part}}. \quad (40)$$

The transverse part of the amplitude can be expressed as

$$\left| \mathcal{M}_{A+B \rightarrow \text{VP}+\phi}^\mu G_T(k, M_\phi) \left(g_{\mu\nu} - \frac{k_\mu k_\nu}{k^2} \right) \mathcal{M}_{\phi \rightarrow \chi\chi}^\nu \right|^2 \quad (41)$$

$$= \left| \sum_{\lambda=\text{T,L}} \mathcal{M}_{A+B \rightarrow \text{VP}+\phi}^\mu G_T(k, M_\phi) (\epsilon_{\lambda,\mu}^* \epsilon_{\lambda,\nu}) \mathcal{M}_{\phi \rightarrow \chi\chi}^\nu \right|^2 \quad (42)$$

$$\rightarrow \frac{1}{3} \sum_{\lambda,\lambda'=\text{T,L}} \left| \left(\mathcal{M}_{A+B \rightarrow \text{VP}+\phi}^\mu \epsilon_{\lambda,\mu}^* \right) G_T(k, M_\phi) \left(\mathcal{M}_{\phi \rightarrow \chi\chi}^\nu \epsilon_{\lambda',\nu} \right) \right|^2. \quad (43)$$

The arrow in Eq. (43) means that decorrelation of polarization structure is valid in calculation of cross section. The validity of decorrelation is shown in Refs. [10]. In the following, we summarize our version (virtual mediator case) of their proof. As in the case of scalar mediator, cross section is written as

$$\hat{\sigma}_{\text{signal}} = \int dm_{\chi\chi}^2 |G_T(m_{\chi\chi}, M_\phi)|^2 \times \frac{1}{2s} \int d\Phi_{\text{VP}} d\Phi_\phi (2\pi)^4 \delta^{(4)} \left(\sum_{i \in \text{ext}} p_i \right) \quad (44)$$

$$\times \frac{1}{2\pi} \int d\Phi_{\text{DM}} (2\pi)^4 \delta^{(4)} \left(p_\phi - \sum_{i \in \text{DM}} p_i \right) \left| \mathcal{M}_{A+B \rightarrow \text{VP}+\phi}^\mu \left(-g_{\mu\nu} + \frac{p_{\phi\mu} p_{\phi\nu}}{p_\phi^2} \right) \mathcal{M}_{\phi \rightarrow \chi\chi}^\nu \right|^2. \quad (45)$$

We assume pair production of dark matter particles and we denote their four momenta by p_1 and p_2 , respectively. If we choose Gottfried-Jackson frame in which $p_\phi = (m_{\chi\chi}, \vec{0})$, then $d\Phi_{\text{DM}} (2\pi)^4 \delta^{(4)}(p_\phi - p_1 - p_2)$ can be replaced by $d\Omega_1 \frac{1}{16\pi^2} \frac{|\vec{p}_1|}{m_{\chi\chi}}$. Also, the spatial component of $\mathcal{M}_{\phi \rightarrow \chi\chi}^\mu$ has to be proportional to \vec{p}_1 since no other vector quantities are involved in the decay process (i.e. $\vec{\mathcal{M}}_{\phi \rightarrow \chi\chi} \propto \vec{p}_1$). $\vec{\mathcal{M}}_{A+B \rightarrow \text{VP}+\phi}^\mu$ does not depend on \vec{p}_1 and \vec{p}_2 and thus we can choose $\theta_1 = \angle(\vec{\mathcal{M}}_{A+B \rightarrow \text{VP}+\phi}^\mu, \vec{p}_1)$ by rotation of the frame. Furthermore, in the Gottfried-Jackson frame, $-g_{\mu\nu} + \frac{p_{\phi\mu} p_{\phi\nu}}{p_\phi^2} = \text{diag}(0, \mathbf{1}_3)$. Thus, eq. (45) becomes

$$\frac{1}{2\pi} \int d\phi_1 \frac{1}{16\pi^2} \frac{|\vec{p}_1|}{m_{\chi\chi}} \int_{-1}^1 d \cos \theta_1 |\vec{\mathcal{M}}_{A+B \rightarrow \text{VP}+\phi}^\mu|^2 |\vec{\mathcal{M}}_{\phi \rightarrow \chi\chi}^\mu|^2 \cos^2 \theta_1 \quad (46)$$

$$= \frac{1}{2\pi} \int d\phi_1 \frac{1}{16\pi^2} \frac{|\vec{p}_1|}{m_{\chi\chi}} \int_{-1}^1 d \cos \theta_1 \frac{1}{3} |\vec{\mathcal{M}}_{A+B \rightarrow \text{VP}+\phi}^\mu|^2 |\vec{\mathcal{M}}_{\phi \rightarrow \chi\chi}^\mu|^2. \quad (47)$$

Finally,

$$|\vec{\mathcal{M}}_{A+B \rightarrow \text{VP}+\phi}^\mu|^2 |\vec{\mathcal{M}}_{\phi \rightarrow \chi\chi}|^2 = \sum_\lambda \left(\mathcal{M}_{A+B \rightarrow \text{VP}+\phi}^\mu(\epsilon_{\lambda,\mu}^* \epsilon_{\lambda,\nu}) \mathcal{M}_{A+B \rightarrow \text{VP}+\phi}^{\nu*} \right) \sum_{\lambda'} \left(\mathcal{M}_{\phi \rightarrow \chi\chi}^\alpha(\epsilon_{\lambda',\alpha}^* \epsilon_{\lambda',\beta}) \mathcal{M}_{\phi \rightarrow \chi\chi}^{\beta*} \right) \quad (48)$$

proves that the decorrelation of polarization is valid.

On the other hand, the longitudinal part in Eq. (40) usually becomes zero. If dark matter particles are scalar field, then $\mathcal{M}_{\phi \rightarrow \chi\chi}^\nu$ is proportional to $(p_1 - p_2)^\nu$ and $p_{\phi\nu} \mathcal{M}_{\phi \rightarrow \chi\chi}^\nu \propto (m_1^2 - m_2^2)$. For fermionic dark matter, we define the vertex function Γ_μ by $\mathcal{M}_{\phi \rightarrow \chi\chi}^\mu \propto \bar{u}_1 \Gamma^\mu v_2$. If $\Gamma^\mu \propto \gamma^\mu$, then $p_{\phi\mu} \mathcal{M}_{\phi \rightarrow \chi\chi}^\mu \propto m_1 - m_2$. If the dark matter particle has other type of interactions with vector mediator (*e.g.*, $\Gamma^\mu \propto \gamma^5 \gamma^\mu$), the proof given in this material is not valid.